ISSN 1674-1056
http://cpb.iphy.ac.cn
http://iopscience.iop.org/cpb
中国物理 B
Chinese Physics
中国物理 Chinese Physics B

Generation of few-cycle radially-polarized infrared pulses in a gas-filled hollow-core fiber

Rui-Rui Zhao(赵睿睿), Zhi-Yuan Huang(黄志远), Ding Wang(王丁), Yu Zhao(赵钰), Yu-Xin Leng(冷雨欣), Ru-Xin Li(李儒新)

Citation: Chin. Phys. B . 2018, 27(10): 104204. **doi:** 10.1088/1674-1056/27/10/104204

Journal homepage: http://cpb.iphy.ac.cn; http://iopscience.iop.org/cpb

What follows is a list of articles you may be interested in

Study on polarization properties of graphene coated D-shaped fiber

Xuejing Liu(刘学静), Luwen Yang(杨禄文), Jingyun Ma(马敬云), Caili Li(李彩丽), Wa Jin(金娃), Weihong Bi(毕卫红)
Chin. Phys. B . 2018, 27(10): 104206. **doi:** 10.1088/1674-1056/27/10/104206

Generation of few-cycle radially-polarized infrared pulses in a gas-filled hollow-core fiber

Rui-Rui Zhao(赵睿睿), Zhi-Yuan Huang(黄志远), Ding Wang(王丁), Yu Zhao(赵钰), Yu-Xin Leng(冷雨欣), Ru-Xin Li(李儒新)
Chin. Phys. B . 2018, 27(10): 104204. **doi:** 10.1088/1674-1056/27/10/104204

Linear polarization output performance of Nd: YAG laser at 946 nm considering the energy-transfer upconversion

Jin-Xia Feng(冯晋霞), Yuan-Ji Li(李渊骥), Kuan-Shou Zhang(张宽收)
Chin. Phys. B . 2018, 27(7): 074211. **doi:** 10.1088/1674-1056/27/7/074211

Wideband linear-to-circular polarization conversion realized by a transmissive anisotropic metasurface

Bao-Qin Lin(林宝勤), Jian-Xin Guo(郭建新), Bai-Gang Huang(黄百钢), Lin-Bo Fang(方林波), Peng Chu(储鹏), Xiang-Wen Liu(刘湘雯)
Chin. Phys. B . 2018, 27(5): 054204. **doi:** 10.1088/1674-1056/27/5/054204

Double-rod metasurface for mid-infrared polarization conversion

Yang Pu(蒲洋), Yi Luo(罗意), Lu Liu(刘路), De He(何德), Hongyan Xu(徐洪艳), Hongwei Jing(景洪伟), Yadong Jiang(蒋亚东), Zhijun Liu(刘志军)
Chin. Phys. B . 2018, 27(2): 024202. **doi:** 10.1088/1674-1056/27/2/024202

Generation of few-cycle radially-polarized infrared pulses in a gas-filled hollow-core fiber*

Rui-Rui Zhao(赵睿睿)[1,2], Zhi-Yuan Huang(黄志远)[1], Ding Wang(王丁)[1,†], Yu Zhao(赵钰)[1,2], Yu-Xin Leng(冷雨欣)[1,‡], and Ru-Xin Li(李儒新)[1]

[1] *State Key Laboratory of High Field Laser Physics, Shanghai Institute of Optics and Fine Mechanics, Chinese Academy of Sciences, Shanghai* 201800, *China*

[2] *University of Chinese Academy of Sciences, Beijing* 100049, *China*

(Received 18 May 2018; revised manuscript received 5 July 2018; published online 10 September 2018)

We perform a numerical study for temporally compressing radially-polarized (RP) infrared pulses in a gas-filled hollow-core fiber (HCF). The dynamic transmission and nonlinear compression of RP pulses centered at wavelengths of 0.8 μm, 1.8 μm, 3.1 μm, and 5.0 μm in HCFs are simulated. By comparing the propagation of pulses with the same optical cycles and intensity, we find that under proper conditions these pulses can be compressed down to 2–3 cycles. In the transverse direction, the spatiotemporal beam profile ameliorates from 0.8-μm to 1.8-μm and 3.1-μm pulses before the appearance of high-order dispersion. These results show an alternative method of scaling generation for delivering RP infrared pulses in gas-filled HCFs, which can obtain energetic few-cycle pulses, and will be beneficial for relevant researches in the infrared scope.

Keywords: pulse compression, polarization, infrared pulses, hollow-core fibers

PACS: 42.65.–k, 42.65.Re, 42.65.Jx, 42.81.Qb **DOI:** 10.1088/1674-1056/27/10/104204

1. Introduction

Radially-polarized (RP) beams have attracted a great deal of interest due to their specific properties. They are exploited in a variety of applications, such as optical trapping and manipulating nanoparticles, microscopy, lithography, frequency shifting, laser processing, and so on.[1] Compared to those with linear polarization (LP) or other circular polarization, one significant advantage of RP beams is tight focusing, which leads to a relatively strong field intensity along the longitudinal direction at the focal region, thus enabling both the pulse duration and peak power to be promoted to a high level of a few optical cycles and gigawatt.[2] Because the high-harmonic generation (HHG) cut-off energy can be scaled as $I\lambda^2$, where I is the field intensity and λ is the radiation wavelength, the search for generating high-power ultrafast pulses in the infrared region has experienced rapid technological advancements.[3,4] Longer wavelengths present better phase-matching conditions for harmonic generation, broader filaments, and more efficient self-steepening characteristics.[5] Till now, optical parametric amplification (OPA) is typically a powerful and reliable approach to produce broadband tunable femtosecond laser pulses in the near-infrared (NIR) or even mid-infrared (MIR) region at moderate energies, taking advantage of the different frequency generation technique in general. Cardin *et al.*[6] compressed the ∼ 11 mJ, 35-fs OPA laser source at 1.8 μm into 5 mJ, 12 fs. The group of Haakestad obtained intense MIR pulses in the 3 μm–5 μm wavelength region with up to 33-mJ high energy.[7]

Over the years, there have been a variety of methods for generating RP pulses such as using polarization converters like liquid crystal spatial light modulators,[8] holographic elements,[9] etc. Recently, an efficient generation of such pulses by combining a gas-filled hollow-core fiber (HCF) with a suitable polarization mode converter has been put forward,[10] which achieved less than 0.9-mJ, ∼ 3-cycle RP beams at 800 nm.[2] This simple approach can be extended to produce RP pulses with a high degree of polarization purity centered at various wavelengths. The noble gas-filled HCF compressor is a universal method of delivering high-energy few-cycle pulses based on the self-phase modulation (SPM) effect.[11,12] However, to the best of our knowledge, spatiotemporal propagation dynamics of RP beams in a gas-filled HCF has rarely been reported so far. In our previous work, Wang *et al.*[13] used a 1-m-long, 500-μm-diameter HCF filled with 0.2 mbar–689.3 mbar (1 bar = 10^5 Pa) argon to explore the direct spectral broadening of RP pulses centered at 800 nm. The propagation differences of LP and RP pulses at the same conditions were compared, showing that it was feasible to broaden RP pulses in gas-filled HCFs, and after HCFs the spatial uniformity of RP pulses was even better than LP pulses, which

*Project supported by the National Natural Science Foundation of China (Grant No. 61521093), the Strategic Priority Research Program of the Chinese Academy of Sciences (Grant No. XDB16), the International S & T Cooperation Program of China (Grant No. 2016YFE0119300), and the Program of Shanghai Academic/Technology Research Leader, China (Grant No. 18XD1404200).

†Corresponding author. E-mail: wangding@siom.ac.cn

‡Corresponding author. E-mail: lengyuxin@mail.siom.ac.cn

© 2018 Chinese Physical Society and IOP Publishing Ltd

resulted in better focusing. On the other hand, there is a lack of understanding about propagation behaviors of femtosecond RP pulses with longer central wavelengths. Considering the excellent properties of infrared pulses, it is required to investigate RP pulses in the NIR and MIR regions propagating in gas-filled HCFs, which would be desirable and beneficial.

In this work, we theoretically study the nonlinear propagation of RP pulses in gas-filled HCFs centered at several typical wavelengths, covering from 0.8 μm to 5.0 μm. Emphasis is put on the numerical propagating results, in which the pulse field is acquired along both the propagating and transverse radial directions, thus we are able to capture the full spatiotemporal dynamics overall. By comparing the results of pulses with the same 15 optical cycles and light intensity centered at different common NIR and MIR wavelengths 0.8 μm, 1.8 μm, 3.1 μm, and 5.0 μm, we find that these pulses can all be compressed to 2–3 cycles under proper conditions. In the transverse direction, the spatiotemporal beam profile ameliorates from 0.8-μm to 1.8-μm, and 3.1-μm pulses before the appearance of high-order dispersion. It is found that the spectral broadening factor becomes larger with the increase of the central wavelength, indicating that a broader spectrum can be achieved for longer wavelengths within certain limits. The use of large-core HCFs is also analyzed, which supports high pulse transmission in the MIR with good beam quality, proving that this method is feasible and robust. In contrast, the method of keeping the same initial full width at half maximum (FWHM) and energy for the scaling generation in the infrared region is relatively difficult to obtain high-energy ultrashort RP pulses. The remainder of this paper is organized as follows. Section 2 briefly introduces the theoretical model. Section 3 presents simulation results for RP pulses centered at 0.8 μm, 1.8 μm, 3.1 μm, and 5.0 μm propagating in argon gas-filled HCFs. Section 4 discusses the case for 3 μm–5 μm MIR pulses in large-core HCFs and compares it with another generation method. The paper ends with a conclusion in Section 5.

2. Theoretical model

Assuming that the beam propagation is of cylindrical symmetry in the simulations, the mathematical model is based on the generalized unidirectional pulse propagation equations (gUPPE-b)[14–16]

$$\partial_z E(z,r,\omega) = \mathrm{i}\left(\sqrt{\hat{L}}-\frac{\omega}{v_\mathrm{g}}\right)E(z,r,\omega) + \frac{\omega}{2\beta c^2}\left[\mathrm{i}\omega\frac{P(z,r,\omega)}{\varepsilon_0}-\frac{j(z,r,\omega)}{\varepsilon_0}\right], \quad (1)$$

where $E(z,r,\omega)$ is the pulse field envelope in the frequency domain; $\hat{L}=\omega^2\varepsilon(\omega)/c^2+\Delta_\perp$ is the linear operator which describes both dispersion and diffraction effects; v_g is the velocity of the moving frame; $\beta=\omega n(\omega)/c$ is the frequency-dependent wavenumber; $P(z,r,\omega)$ describes the nonlinear polarizations related to bound and free electrons; $j(z,r,\omega)$ is the description of plasma effects; and ω, c, and ε_0 are angular frequency, light speed, and vacuum permittivity, respectively. The nonlinear polarization for the temporal cubic Kerr effect is $P/\varepsilon_0=2n_0n_2\mathcal{I}E$, where $\mathcal{I}=|E|^2$ is the optical pulse intensity envelope. Free electrons are born to introduce a current density $j(t)$ in the time domain when the gas medium in HCFs is ionized. Thus the gas ionization effect can be modeled by $j(t)/\varepsilon_0=cn_0W(\mathcal{I})U_\mathrm{i}(\rho_\mathrm{nt}-\rho)E/\mathcal{I}$, where $W(\mathcal{I})$ is the ionization rate calculated according to the Perelomov–Popov–Terentiev (PPT) model,[17] which is illustrated in Fig. 1 as a function of the pulse intensity; U_i is the ionization potential; ρ is the electron density; and ρ_{nt} is the neutral density of the gas. The plasma effect in the frequency domain is modeled by

$$j(\omega)/\varepsilon_0=\frac{\tau_\mathrm{c}(1+\mathrm{i}\omega\tau_\mathrm{c})}{1+\omega^2\tau_\mathrm{c}^2}\frac{e^2}{\varepsilon_0 m_\mathrm{e}}\mathrm{FFT}[\rho E],$$

where e, m_e, and τ_c are the electron charge, mass, and collision time, respectively. Supposing that the ionized electrons are created at rest, the electron density ρ evolves as

$$\partial_t\rho=W(\mathcal{I})(\rho_\mathrm{nt}-\rho)+\sigma\mathcal{I}\rho/U_\mathrm{i}, \quad (2)$$

where σ is the impact ionization cross section.

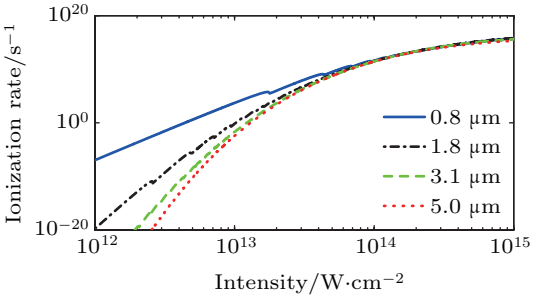


Fig. 1. (color online) PPT ionization rate versus pulse intensity in argon for different central wavelengths.

For the propagation of RP pulses in HCFs, there are two main boundary conditions: firstly, the field on the central axis is null, namely $E_\mathrm{axis}=0$;[18] secondly, the field at the intersection of gas and fiber clad is $E_\mathrm{intersection}=(4E_1-E_2)/(3-2\mathrm{i}k_\mathrm{clad}\Delta r/n_\mathrm{clad}^2)$, where E_1 and E_2 are fields at Δr and $2\Delta r$ away from the boundary of the hollow core; k_clad and n_clad are the wavenumber and linear refractive index of the fiber clad. The envelope of the initial pulse generally takes the form as

$$E(z=0,t,r)=E_0 f(r)\exp\left\{-\frac{r^2}{w_0^2}\right\}\exp\left\{-\frac{t^2}{2t_0^2}\right\}, \quad (3)$$

where E_0, w_0, and t_0 are the initial amplitude, beam waist, and duration of the input pulse, respectively; $f(r)=1$ indicates

that the pulse is Gaussian in the spatial domain and $f(r) = r$ corresponds to the profile of RP pulses.[1]

For nonlinear compression in HCFs, the optimal coupling condition for RP pulses focused into HCFs is when the beam waist occupies half of the fiber radius, namely $w_0 = 0.5a$.[13] Besides, the energy efficiency is also an important point. In the hollow waveguide, the linear attenuation coefficient of the laser field can be described as

$$\alpha_m = \left(\frac{U_m}{2\pi}\right)^2 \frac{\lambda^2}{a^3} \frac{\nu^2+1}{2\sqrt{\nu^2-1}}, \tag{4}$$

where U_m is the m-th zero point of a zero-order Bessel function of the first kind; λ is the wavelength; a is the fiber radius; and ν is the ratio of refractive indices of the fiber clad and fiber core. The spectral broadening is mainly achieved by SPM that relates to the group velocity dispersion parameter β_2. Figure 2 shows the power attenuation and β_2 of the fundamental mode for three different typical HCF inner diameters with respect to the wavelength ranging from 0.5 μm to 5.7 μm. For a 250-μm-diameter HCF, the waveguide loss is large, and there is a significant rising trend for longer wavelengths. Both the attenuation coefficient and β_2 value stay modest in a 500-μm-diameter HCF. Although there is nearly no power loss in a 1000-μm HCF, β_2 remains almost zero over all wavelengths, which is not conducive for pulse temporal compression. Therefore, setting the HCF diameter to be 500 μm for NIR and MIR pulses is relatively superior.

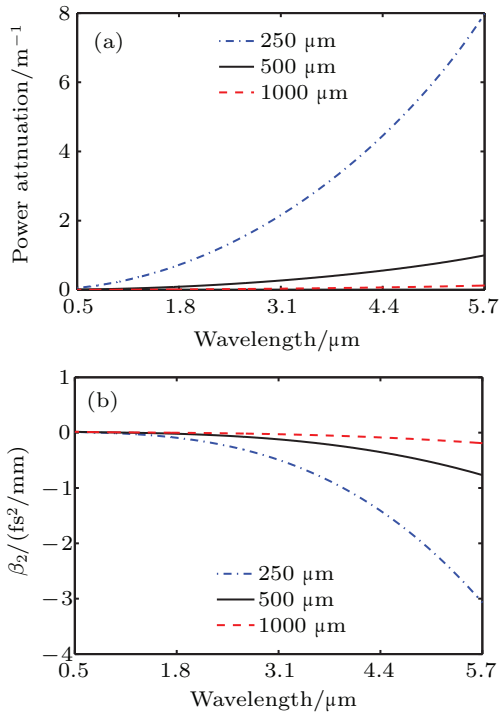


Fig. 2. (color online) (a) Linear attenuation and (b) β_2 for different wavelengths ranging from 0.5 μm–5.7 μm.

3. Simulation results

Based on the theoretical model above, we present the numerical results. Here a 500-μm-inner-diameter, 1-m-long argon gas-filled HCF is employed, which is widely used in practice.[19] In order to mimic the real common experimental conditions,[2] the simulation parameters are set as follows. For RP pulses centered at 0.8 μm, the initial energy and duration are 1.5 mJ and 40 fs, respectively. In the gas pressure-gradient method which can suppress undesirable high-order modes in HCFs, the pressure is gradually increased with the pulse propagation distance as $p(x) = \sqrt{p_{\text{in}}^2 + x(p_{\text{out}}^2 - p_{\text{out}}^2)/L}$,[20] where p_{in} and p_{out} are gas pressures at the fiber inlet and outlet, respectively, L is the fiber length, and x is the propagation distance. Here p_{in} is set to be 2 mbar, which corresponds to the lowest pressure obtained by the lab pump; p_{out} is set to be 610 mbar, where the accumulated nonlinearity for pressure-gradient implementation is the same as that for the $p = 440$ mbar static pressure case. The critical power for self-focusing is $P_{\text{cr}} = \lambda_0^2/(2\pi n_2)$, where n_2 is the nonlinear index coefficient, so here the initial power ratio $P_{\text{in}}/P_{\text{cr}}$ is equal to 0.81. To preserve the same initial light intensity for longer wavelengths, the power ratio needs to be reduced, while the pressure should be enhanced proportionally. On the other side, the initial pulse cycle is kept the same, i.e., 15 optical cycles. For RP 1.8-μm pulses, we fix this ratio $P_{\text{in}}/P_{\text{cr}} = 0.73$ with a pressure-gradient of 2 mbar–1390 mbar (analogous to 1000-mbar static pressure). For RP 3.1-μm pulses, $P_{\text{in}}/P_{\text{cr}} = 0.41$ with a pressure-gradient of 2 mbar–2390 mbar (analogous to 1720-mbar static pressure). Pulses centered at 5.0 μm with radial polarization take a high gas pressure, with a pressure-gradient of 2 mbar–3860 mbar (analogous to 2780-mbar static pressure), corresponding to a small power ratio $P_{\text{in}}/P_{\text{cr}} = 0.19$. However, because the output pulse centered at 5.0 μm splits severely when the initial energy is 9.0 mJ as calculated, in order to guarantee no pulse breakup, we gradually reduce its energy and find that the optimal condition meets the initial energy of 7.0 mJ. Note that the Kerr index coefficient is chosen within a narrow value interval: for $\lambda_0 = 0.8$-μm pulses, the well-known nonlinear index $n_2 = p \times 10^{-19}$ cm^2/W is utilized;[21–23] for $\lambda_0 \geq 2$ μm, n_2 needs to have values close to $0.97p \times 10^{-19}$ cm^2/W, as proposed before.[24] Since the ratio p/λ_0 is held constant, in consequence, the chromatic dispersion does not change much and indeed approaches normal for the 0.8 μm–5.0 μm infrared wavelength region. Table 1 shows the RP input-pulse parameters for different central wavelengths.

Figure 3 shows the evolution of the normalized energies for 0.8-μm, 1.8-μm, 3.1-μm, and 5.0-μm pulses with radial polarization along the propagation. Here the gUPPE-b model

is an improved method based on expansion of the propagating field into approximate leaky waveguide modes, which can correctly compute the energy loss through the waveguide wall and definitely simulate various nonlinear optics in the MIR region.[14] Thus, the acquired outcome is more accurate. It can be seen that the energy of pulses centered at 0.8 μm, 1.8 μm, and 3.1 μm decreases smoothly with a slower speed, close to a straight line. For 5.0 μm pulses, the energy efficiency diminishes significantly, and even reduces to less than 30% when transporting a 1-m-long distance. With the increase of the pulse central wavelength, the transmission ratio falls off faster, which is mainly due to more multi-photon absorption and ionization boosting loss. Longer infrared wavelengths were not explored, because the output-pulse energy is much lower, thus further increasing the wavelength would be meaningless for real experiments.

Table 1. Input-pulse parameters for different wavelengths.

Wavelength/μm	Input duration/fs	Input energy/mJ	Gas pressure/mbar
0.8	40	1.5	2–610 (static: 440)
1.8	90	3.5	2–1390 (static: 1000)
3.1	155	6.0	2–2390 (static: 1720)
5.0	250	9.0 (reduced to 7.0)	2–3860 (static: 2780)

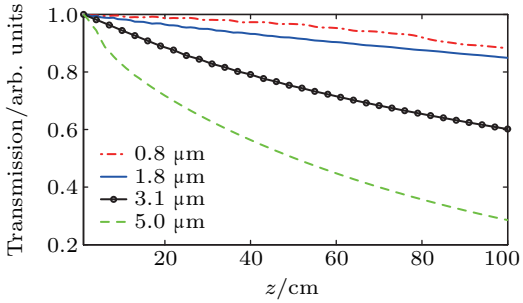


Fig. 3. (color online) Energy transmission along the propagation in HCFs.

Figure 4 shows the compensated RP pulse temporal and spectral intensity profiles after integrating the radial envelope. It is found that using the -56 fs^2 group delay dispersion (GDD) compensation can compress the 0.8 μm pulses to 2.4 optical cycles (6.4 fs). Due to the anomalous dispersion at long wavelengths above 1.3 μm, the chirp compensation is usually done with ordinary bulk materials such as CaF_2 crystal. For 1.8-μm, 3.1-μm, and 5.0-μm compressed pulses, the number of optical cycles can be achieved down to 3.0 (18.2 fs), 2.2 (22.6 fs), and 2.0 (32.8 fs), with the optimal CaF_2 thickness of 5 mm, 4 mm, and 0.6 mm, respectively. Therefore, the temporal compression ratio is calculated as 6.0, 4.9, 6.9, and 7.6, respectively. Moreover, the pulse profile after optimal GDD or CaF_2 compensation is analogous to the Fourier-transform limited (FTL) profile for 0.8-μm, 1.8-μm, and 3.1-μm pulses, illustrating that there is no need to use higher-order dispersion for the compensation. However, due to the generation of more high-order dispersion for longer wavelengths, for 5.0-μm pulses, only using CaF_2 compensation cannot compress its profile to the FTL profile.

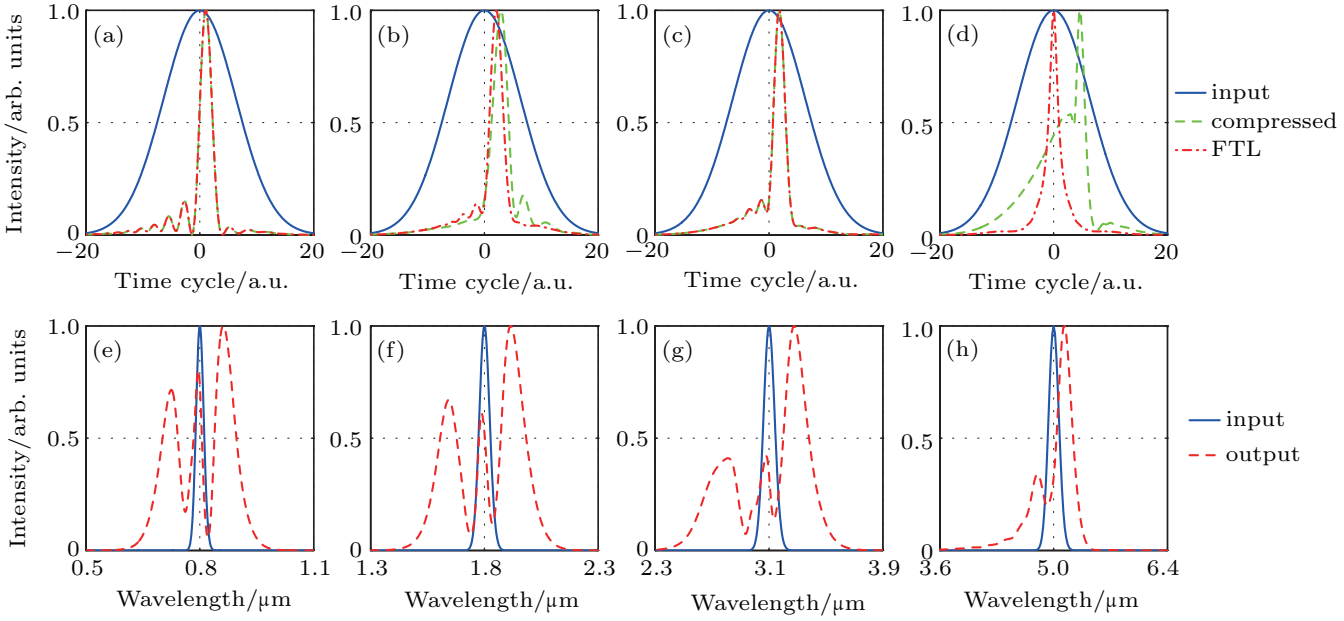


Fig. 4. (color online) Total intensity profiles for input and output RP pulses with different central wavelengths in (a)–(d) time and (e)–(h) frequency domains: (a) and (e) 0.8 μm, (b) and (f) 1.8 μm, (c) and (g) 3.1 μm, and (d) and (h) 5.0 μm.

The evolution of the transverse energy distribution for 0.8-μm, 1.8-μm, 3.1-μm, and 5.0-μm pulses with radial polarization is shown in the first row of Fig. 5. It can be seen that for pulses centered at 0.8 μm, the transverse distribution exhibits irregularity, while for longer wavelengths the transverse distribution becomes stable and smooth. The main reason is that the ratio $P_{\rm in}/P_{\rm cr}$ decreases. Because gUPPE-b is a function of the fiber radius where the pulse envelopes differ at different radii, the total spectrum in the second row of Fig. 5 is obtained by integrating along the fiber radial direction, which is more precise than other cases excluding the fiber radius. Before the 50-cm propagation where the gas pressure is relatively low, almost all of the spectra are not broadened; after 50 cm the spectral broadening is enhanced with the increase of the wavelength. Note that the red-shift is obviously more intense in the spectrum with the central wavelength increasing, owing to the stronger nonlinearity.

Figure 6 further reveals the temporal and spectral distribution for 0.8-μm, 1.8-μm, 3.1-μm, and 5.0-μm pulses with radial polarization at the outlet of HCF before compression. With the increase of the central wavelength, it can be seen that the beam size enlarges gradually along the fiber radial direction. The beam profile ameliorates for 1.8-μm and 3.1-μm pulses, which is more symmetric and smooth in the time domain; while for pulses with longer wavelength 5.0 μm, the profile deteriorates as high-order dispersion occurs. It is interesting to notice that with the central wavelength increasing, there is a little more spatial chirp in the short wavelength range of the spectrum, resulting from stronger nonlinear interactions such as self-steepening, ionization, and plasma effects which induce asymmetry. After proper chirp compensation, the FWHM of the output pulse can be temporally compressed to a smaller value, and the pulse envelope is preferable as there is a dominant peak.

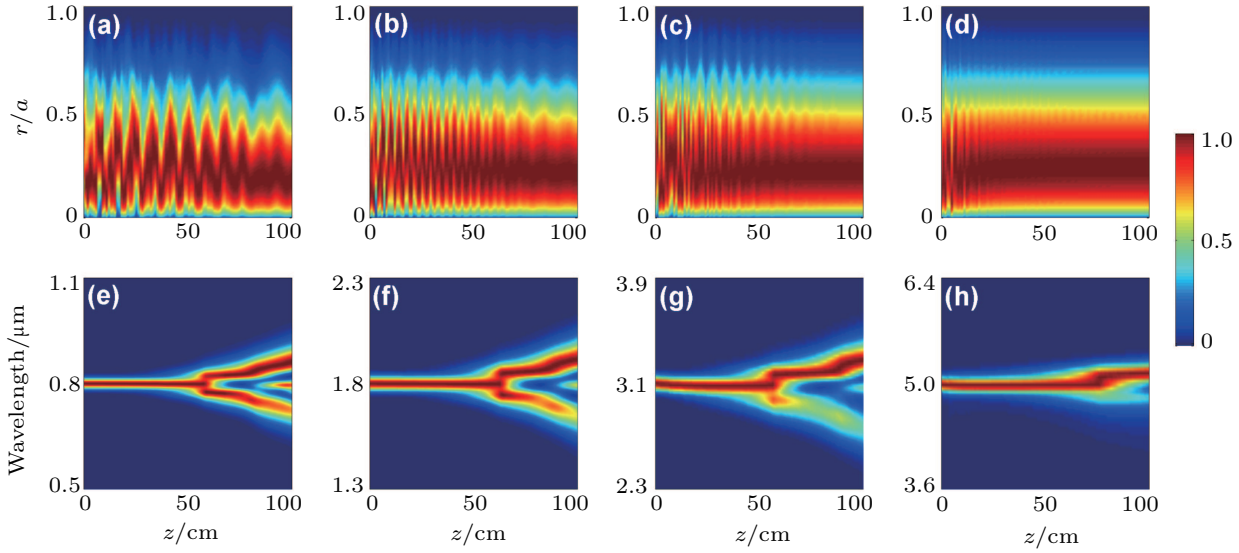


Fig. 5. (color online) Total (a)–(d) transverse energy distribution and (e)–(h) spectral propagation dynamics with transmitting distances for RP pulses at different central wavelengths: (a) and (e) 0.8 μm, (b) and (f) 1.8 μm, (c) and (g) 3.1 μm, and (d) and (h) 5.0 μm.

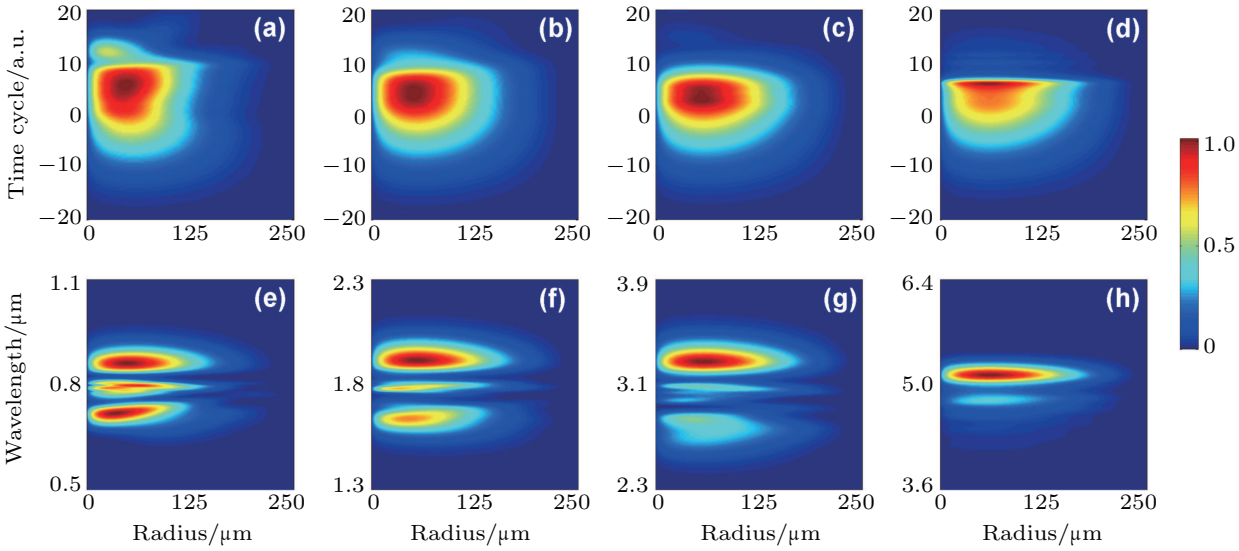


Fig. 6. (color online) The output-pulse (a)–(d) temporal and (e)–(h) spectral distribution along the fiber radial direction before compression for RP pulses with different central wavelengths: (a) and (e) 0.8 μm, (b) and (f) 1.8 μm, (c) and (g) 3.1 μm, and (d) and (h) 5.0 μm.

To distinctly compare the ability of spectral broadening in the infrared region, here the root-mean-square (RMS) method is employed. The broadening factor δ can be described as $\delta = \Delta\omega_{\rm rms}/\Delta\omega_0$, where $\Delta\omega_{\rm rms}$ and $\Delta\omega_0$ are the RMS spectral widths of the output and input pulses, respectively, which can also be written as[25,26]

$$\begin{cases} (\Delta\omega)^2 = \langle(\omega-\omega_0)^2\rangle - \langle(\omega-\omega_0)\rangle^2, \\ \langle(\omega-\omega_0)^n\rangle = \dfrac{\int_{-\infty}^{\infty}(\omega-\omega_0)^n I(\omega)\,\mathrm{d}\omega}{\int_{-\infty}^{\infty} I(\omega)\,\mathrm{d}\omega}, \end{cases} \tag{5}$$

where $I(\omega)$ is the spectral intensity; ω_0 is obtained by $\omega_0 = \int_{-\infty}^{\infty}\omega I(\omega)\,\mathrm{d}\omega / \int_{-\infty}^{\infty} I(\omega)\,\mathrm{d}\omega$.

Spectral broadening is identified mainly through observing the change of the broadening factor δ of the output RP pulses with the central wavelength increasing. The larger δ is, the wider the spectrum broadens.

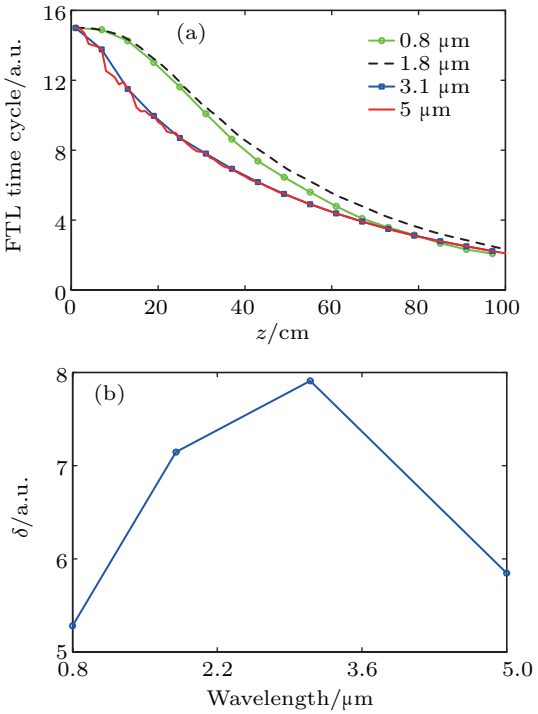


Fig. 7. (color online) (a) The FTL pulse optical cycle along the propagation; (b) output-pulse broadening factor at different wavelengths.

Figure 7(a) shows the evolution of FTL optical cycles for 0.8-μm, 1.8-μm, 3.1-μm, and 5.0-μm pulses with radial polarization. In the transmitting process, all the pulse cycles show a smooth and uniform change, except that there is a quicker decreasing speed in the cycle lines of 3.1 μm and 5.0 μm at the very beginning. The spectral broadening factor δ of output RP pulses with increasing central wavelengths is shown in Fig. 7(b). Note that the spectrum starts to broaden before the 3.1 μm wavelength, but after that it shows a narrower trend. This illustrates the weaker SPM effect for the 5.0-μm pulse, which is mainly due to the very low transmission ratio in Fig. 3, resulting in insufficient interactions between pulses and noble gases as well as inferior spectral broadening.

4. Discussions

It can be seen in Fig. 2(a) that using HCFs with larger diameter for longer central wavelength pulses could reduce loss, and the critical reason for the small broadening factor of 5.0-μm pulses in Fig. 7(b) is the very large attenuation. Thus, we employ a 1000-μm-inner-diameter HCF to study the spectral broadening for 3 μm–5 μm MIR pulses with radial polarization. In our previous work, Wang *et al.*[27] experimentally demonstrated the generation of 2.6 mJ, ∼ 1.6 cycle laser pulses at 4-μm central wavelength, by spectral broadening of the pulse through a 1-mm-diameter, 3-m-long HCF filled with ∼ 1.2-bar krypton and the dispersion compensation. Therefore, the initial energy and duration of the RP pulses centered at 4.0 μm are set to 5.0 mJ and 10 optical cycles (∼ 135 fs), the same input parameters as the common experimental work.[27] To preserve a high transmission, the 1000-μm-diameter krypton gas-filled HCF is selected to be 1-m long. By adjusting the gas pressure, it is found that the optimal krypton pressure gradient is 2 mbar–2080 mbar (analogous to 1500-mbar static pressure). According to the above-described method, the initial light intensity and optical cycles are kept the same for 3.1-μm and 5.0-μm pulses with radial polarization, as shown in Table 2.

Table 2. Input-pulse parameters for different wavelengths.

Wavelength/μm	Input duration/fs	Input energy/mJ	Gas pressure/mbar
3.1	105	4.0	2–1610 (static: 1160)
4.0	135	5.0	2–2080 (static: 1500)
5.0	170	6.5	2–2610 (static: 1880)

Evolutions of normalized total energies during propagation for RP 3.1-μm, 4.0-μm, and 5.0-μm pulses in krypton gas-filled HCFs are shown in Fig. 8(a), where the total-energy efficiency is all above 80%, satisfying the demand for high energy in practice. It can be seen in Fig. 8(b) that the broadening factor δ becomes larger with the increase of the central wavelengths in the 3 μm–5 μm MIR region, indicating that this scaling method can boost spectral broadening for longer wavelengths effectively. For 3.1-μm, 4.0-μm, and 5.0-μm pulses with radial polarization, the temporal intensity profiles

are presented in Figs. 8(c)–8(e), and the number of optical cycles after compensation can attain 2.6 (26.4 fs), 2.4 (31.9 fs), and 2.3 (39.1 fs), with the optimal CaF_2 thickness 3.2 mm, 2.1 mm, and 1.7 mm, respectively. It is interesting to notice that the FTL profile at 5.0 μm shows less asymmetry than that at 3.1 μm, and the corresponding cycle even achieves 0.3 (5.6 fs), because of the stronger nonlinear effects, such as SPM, which are ideal for spectral broadening. This discussion illustrates the robustness of this method.

The spectral broadening of pulses in a noble gas-filled HCF needs to greatly take into account the energy transmission efficiency. The longer the laser wavelength is, the larger the waveguide attenuation is. For long-wavelength pulses, the large-core HCF should be employed, which would reduce the decent function on filtering modes. On the other hand, under the current experimental conditions, the largest diameter of HCF is 1000 μm. The energy transmission for 10-μm pulses in a 1000-μm-inner-diameter HCF is calculated below 50% according to Eq. (4), which is unacceptable in the experiments. Therefore, infrared pulses centered at 0.8-μm, 1.8-μm, 3.1-μm, and 5.0-μm wavelengths that are typical and common in practice are studied in this work.

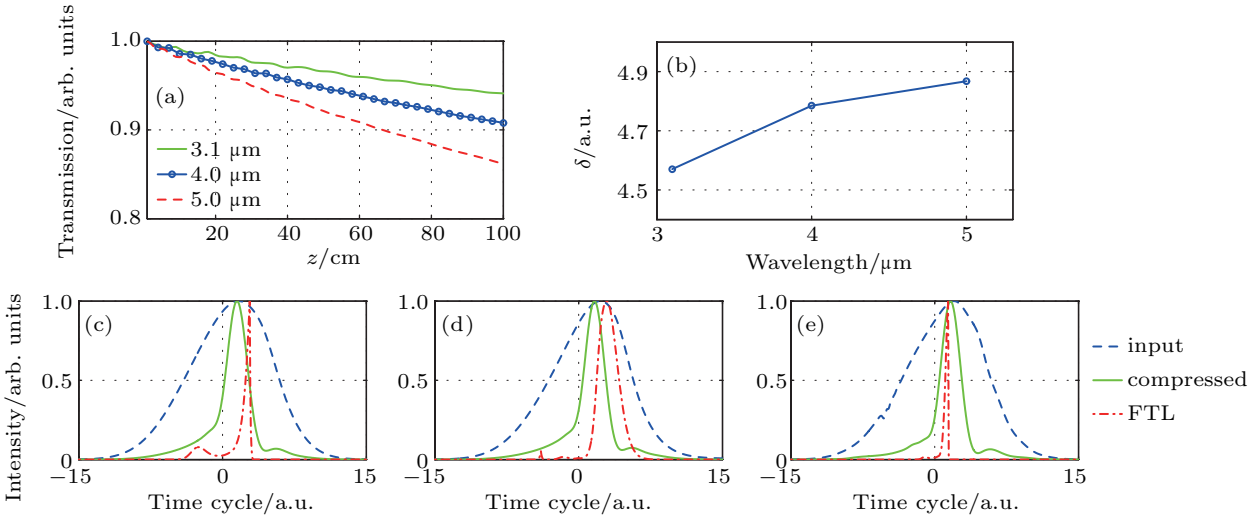


Fig. 8. (color online) (a) Energy transmission along the propagation; (b) output-pulse broadening factor at different wavelengths; (c)–(e) total temporal intensity profiles for RP 3.1-μm, 4.0-μm, and 5.0-μm pulses.

Because the broadening factor δ is related to the intensity and loss of the input pulses, we also numerically study how the spectrum is broadened in the case of 40 fs initial duration and 1.5 mJ initial energy for 0.8-μm, 1.8-μm, 3.1-μm, and 5.0-μm pulses with radial polarization propagating in a 500-μm-inner-diameter, 1-m-long argon gas-filled HCF with a pressure gradient of 2 mbar–610 mbar. For longer wavelength pulses, the waveguide attenuation gets larger, the nonlinear refractive index n_2 becomes smaller, and the ionization rate also diminishes. As a consequence, the method of keeping the same initial FWHM and energy for the scaling generation of NIR and MIR pulses with radial polarization has little capacity to broaden the spectrum, which is relatively difficult to obtain high-energy few-cycle RP pulses compared with the above-described method.

5. Conclusions

We perform a numerical study of generating few-cycle RP infrared pulses in a gas-filled HCF. According to the gUPPE-b model, the dynamic transmission and nonlinear compression of RP pulses centered at 0.8-μm, 1.8-μm, 3.1-μm, and 5.0-μm wavelengths in HCFs are simulated. By comparing the propagation of the pulses with the same dozen optical cycles and intensity, we find that under proper conditions these pulses can be compressed to 2–3 cycles. By using a 500-μm-inner-diameter, 1-m-long argon gas-filled HCF, 0.8 μm/40 fs/1.5 mJ pulses at a static gas pressure of 440 mbar, 1.8 μm/90 fs/3.5 mJ pulses at 1000 mbar, and 3.1 μm/155 fs/6.0 mJ pulses at 1720 mbar can be well compressed to 6.7 fs, 18.2 fs, and 22.6 fs, respectively; that is, 15 optical cycles are compressed to 2–3 cycles. While by using a 1000-μm-inner-diameter, 1-m-long krypton gas-filled HCF, 3.1 μm/105 fs/4.0 mJ pulses at 1160 mbar, 4.0 μm/135 fs/5.0 mJ pulses at 1500 mbar, and 5.0 μm/170 fs/6.5 mJ pulses at 1880 mbar can be well compressed to 26.4 fs, 31.9 fs, and 39.1 fs, respectively; that is, 10 optical cycles are compressed to 2–3 cycles. In the transverse direction, the spatiotemporal beam profile ameliorates from 0.8-μm to 1.8-μm and 3.1-μm pulses before the appearance of high-order dispersion. It is found that the spectral broadening factor becomes larger with the increase of central wavelengths, indicating that a broader spectrum can be achieved for longer wavelengths within certain limits. Using large-core HCFs is able to support high pulse transmission in the MIR region with good beam quality, which proves that this method is feasible and robust. The method of keeping the same initial FWHM and energy for the scaling generation of NIR and MIR

pulses is also studied numerically, with which it is relatively difficult to obtain high-energy ultrashort RP pulses. These results suggest an alternative method of scaling generation for delivering RP infrared pulses in gas-filled HCFs, which can obtain energetic few-cycle pulses, that are beneficial for relevant researches in the infrared scope.

References

[1] Zhan Q 2009 *Adv. Opt. Photon.* **1** 1
[2] Carbajo S, Granados E, Schimpf D, Sell A, Hong K, Moses J and Kartner F X 2014 *Opt. Lett.* **39** 2487
[3] Pogorelsky I V, Yakimenko V, Polyanskiy M, Shkolnikov P, Ispiryan M, Neely D, McKenna P, Carroll D, Najmudin Z and Willingale L 2010 *Nucl. Instrum. Methods Phys. Res. A* **620** 67
[4] Haberberger D, Tochitsky S and Joshi C 2010 *Opt. Express* **18** 17865
[5] Bergé L 2008 *Opt. Express* **16** 21529
[6] Cardin V, Thiré N, Beaulieu S, Wanie V, Légaré F and Schmidt B E 2015 *Appl. Phys. Lett.* **107** 181101
[7] Haakestad M W, Arisholm G, Lippert E, Nicolas S, Rustad G and Stenersen K 2008 *Opt. Express* **16** 14263
[8] Stalder M and Schadt M 1996 *Opt. Lett.* **21** 1948
[9] Churin E G, Hosfeld J and Tschudi T 1993 *Opt. Commun.* **99** 13
[10] Machavariani G, Lumer Y, Moshe I, Meir A and Jackel S 2007 *Opt. Lett.* **32** 1468
[11] Nisoli M, De S and Svelto O 1996 *Appl. Phys. Lett.* **68** 2793
[12] Nisoli M, De S, Svelto O, Szipöcs R, Ferencz K, Spielmann C, Sartania S and Krausz F 1997 *Opt. Lett.* **22** 522
[13] Wang D, Qiao L, Zhao R, Zhao Y and Leng Y 2017 *Opt. Express* **25** 3083
[14] Andreasen J and Kolesik M 2013 *Phys. Rev. E* **87** 053303
[15] Andreasen J and Kolesik M 2012 *Phys. Rev. E* **86** 036706
[16] Kolesik M and Moloney J V 2004 *Phys. Rev. E* **70** 036604
[17] Perelomov A M, Popov V S and Terentév M V 1966 *Sov. Phys. -JETP* **23** 924
[18] Couairon A, Brambilla E, Corti T, Majus D, Ramirez-Gongora O de J and Kolesik M 2011 *Eur. Phys. J. Spec. Top.* **199** 5
[19] Nagy T, Pervak V and Simon P 2011 *Opt. Lett.* **36** 4422
[20] Nurhuda M, Suda A, Midorikawa K, Hatayama M and Nagasaka K 2003 *J. Opt. Soc. Am. B* **20** 2002
[21] Skupin S, Stibenz G, Bergé L, Lederer F, Sokollik T, Schnürer M, Zhavoronkov N and Steinmeyer G 2006 *Phys. Rev. E* **74** 056604
[22] Loriot V, Hertz E, Faucher O and Lavorel B 2009 *Opt. Express* **17** 13429
[23] Loriot V, Hertz E, Faucher O and Lavorel B 2010 *Opt. Express* **18** 3011
[24] Ettoumi W, Petit Y, Kasparian J and Wolf J P 2010 *Opt. Express* **18** 6613
[25] Pinault S C and Potasek M J 1985 *J. Opt. Soc. Am. B* **2** 1318
[26] Agrawal G P 2007 *Nonlinear Fiber Optics* (New York: Elsevier) p. 65
[27] Wang P, Li Y, Li W, Su H, Shao B, Li S, Wang C, Wang D, Zhao R, Peng Y, Leng Y, Li R and Xu Z 2018 *Opt. Lett.* **43** 2197